RESEARCH ARTICLE | MAY 24 2024

Percolation transition and bimodal density distribution in hydrogen fluoride

Elija Feigl; Pál Jedlovszky 💿 ; Marcello Sega 🗷 📵



J. Chem. Phys. 160, 204503 (2024) https://doi.org/10.1063/5.0207202





Articles You May Be Interested In

Markov state model of the two-state behaviour of water

J. Chem. Phys. (October 2016)

The water bimodal inherent structure and the liquid–liquid transition as proposed by the experimental density data

J. Chem. Phys. (May 2024)

Phase diagram of two-dimensional hard ellipses

J. Chem. Phys. (May 2014)





Percolation transition and bimodal density distribution in hydrogen fluoride

Cite as: J. Chem. Phys. 160, 204503 (2024); doi: 10.1063/5.0207202

Submitted: 6 March 2024 • Accepted: 6 May 2024 •

Published Online: 24 May 2024







Elija Feigl,¹ Pál Jedlovszky,² D and Marcello Sega^{3,a)}



AFFILIATIONS

- ¹ Faculty of Physics, University of Vienna, Boltzmanngasse 5, Wien A-1090, Austria
- ²Department of Chemistry, Eszterházy Károly Catholic University, Leányka utca 12, H-3300 Eger, Hungary
- Department of Chemical Engineering, University College London, WC1E 7JE London, United Kingdom
- a) Author to whom correspondence should be addressed: m.sega@ucl.ac.uk

ABSTRACT

Hydrogen-bond networks in associating fluids can be extremely robust and characterize the topological properties of the liquid phase, as in the case of water, over its whole domain of stability and beyond. Here, we report on molecular dynamics simulations of hydrogen fluoride (HF), one of the strongest hydrogen-bonding molecules. HF has more limited connectivity than water but can still create long, dynamic chains, setting it apart from most other small molecular liquids. Our simulation results provide robust evidence of a second-order percolation transition of HF's hydrogen bond network occurring below the critical point. This behavior is remarkable as it underlines the presence of two different cohesive mechanisms in liquid HF, one at low temperatures characterized by a spanning network of long, entangled hydrogenbonded polymers, as opposed to short oligomers bound by the dispersion interaction above the percolation threshold. This second-order phase transition underlines the presence of marked structural heterogeneity in the fluid, which we found in the form of two liquid populations with distinct local densities.

© 2024 Author(s). All article content, except where otherwise noted, is licensed under a Creative Commons Attribution (CC BY) license (https://creativecommons.org/licenses/by/4.0/). https://doi.org/10.1063/5.0207202

INTRODUCTION

Hydrogen fluoride (HF) is one of the strongest hydrogen-bond forming liquids known and a key chemical in essential industrial processes, as a catalyst in alkylation units,1 in the production of aluminum as a precursor of cryolite, 2,3 in the production of organofluorine compounds,4 as well as in silicon wafer etching.5 HF is known to form persistent hydrogen-bonded structures, including linear chains, rings, and branched structures,⁶ and its complex behavior under varying thermodynamic conditions makes it one of the prime candidates for testing our understanding of fluid association. This complexity arises from a combination of the capability to form exceptionally strong hydrogen bonds, the linear nature of the molecule, and its large electronic polarizability, which is crucial in determining several thermodynamic and structural properties, including, for example, a markedly different dipole moment in the liquid and gaseous phases.

The theoretical framework for associating liquids like HF has evolved significantly over the years. Early models focused on

simple associating behaviors, but recent developments in Statistical Associating Fluid Theory (SAFT) and related approaches have provided a more refined understanding of these systems. In theories like Wertheim's, it is not straightforward to incorporate the cooperativity effects in hydrogen bonding or the formation of ring-like structures.⁷ Recent developments have improved our understanding of liquids like HF.^{8–10} Other advances in computational chemistry, particularly molecular dynamics simulations, have provided new avenues for investigating the behavior of HF. Ab initio and empirical models have been instrumental in examining HF's structural and thermodynamic properties, providing insights into its liquid state.11

Much less information is available about the topological characteristics of HF's hydrogen-bonded network. The presence or absence of infinite hydrogen-bond clusters of molecules in an associating fluid can strongly influence its properties and has been linked, for example, to the solubility of small organic compounds, 17 the supercritical behavior of water, ¹⁸⁻²¹ the stability of DNA, ²² as well as the surface tension anomaly of water. 23,24 Å previous analysis by Kolafa and Nezbeda²⁵ shows that primitive models for molecules with asymmetric hydrogen bonding sites, such as ammonia, methanol, or HF, do not predict the formation of percolating hydrogen-bond networks, in contrast to the case of water.

The HF molecule could be in first instance approximated using a dipolar hard sphere model. ^{26,27} However, dipolar hard spheres are now suspected to not admit a liquid-vapor phase transition. ^{28–30} The addition of a Lennard-Jones potential to the dipolar interaction, as in a Stockmayer fluid, ³¹ would seem to be a more appropriate choice to model HF. However, as it was clearly demonstrated by Deraman *et al.*, ³² the structure of liquid HF is markedly different from that of a dipolar fluid, and only the addition of a quadrupole moment reproduces the experimentally determined structure.

Given the rich phenomenology of HF, we aim to investigate the statistics of hydrogen-bond networks in HF with a more refined model, using atomistic molecular dynamics.

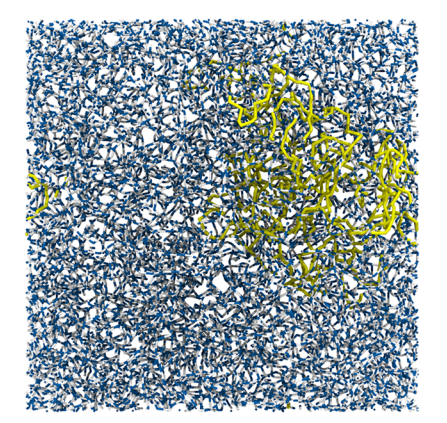
METHODS

The first semiempirical models for liquid HF date back to 1978, when Jorgensen and Cournoyer,³³ and later Klein *et al.*,³⁴ developed early interaction potentials based on *ab initio* calculations. Later, Cournoyer and Jorgensen introduced the three-site HFC model.^{35,36} This model, favoring three-site over two-site configurations, aligned better with the first neutron diffraction experiments on liquid HF reported one year later.³² Another three-site model (JV-NP) was proposed in 1997 by Jedlovszky and Vallauri, which incorporated long-range corrections for Coulomb interactions.³⁷ Although this model performed, in general, better than the previous ones, it failed to replicate the temperature dependence of HF's density and the dimer structure.

In fact, the inability to reproduce the properties of the liquid and vapor phases simultaneously turned out to be a general failure of all non-polarizable models.

For this reason, Jedlovszky and Vallauri introduced a polarizable version of their model (JV-P) to include cooperative effects. The JV-P model showed reasonable accuracy across various thermodynamic states and radial distribution functions in the liquid state, as well as an improved description of the isolated dimer regarding

available experimental³⁹ and *ab initio* results.⁴⁰ In particular, later experiments by Pfeiderer et al. 41 proved the model's ability to reproduce the elongation of the hydrogen bond that occurs when moving from the liquid to the gas phase.⁴² In response to new experimental measurements on partial structure factors in a broad range of thermodynamic states, ^{43,44} Pártay, Jedlovszky, and Vallauri introduced the PJV-P model, ¹¹ essentially a complete reparameterization of JV-P to match the newly available experimental data. The PJV-P model forms the foundation for the model used in this work. The original PJV-P model represented the polarizability using an induced point-dipole, which required an iterative, self-consistent field (SCF) procedure for accurate determination, and long-range contributions were taken into account using the reaction field method. This approach was especially effective for Monte Carlo (MC) simulations involving minimal perturbations to the system. However, induced dipoles necessitated additional handling beyond point charge interactions, a feature not inherently supported by common atomistic MD simulation packages. We adapted the PJV-P model by replacing the point dipole with a Drude oscillator and treated long-range contribution using the smooth Particle Mesh Ewald (sPME) algorithm. In this adaptation, which we call PJVP-Drude (PJVP-D), a Drude charge (q_D) was positioned on the Drude site (D), with the fluorine (F) site's charge adjusted to preserve overall neutrality. The Drude charge was connected to the fluorine via a harmonic spring potential, forming an oscillating dipole. In principle, one can recover the limit of a point dipole when polarization charge q_D and spring constant $k_{\rm D}$ are infinitely large in such a way that the polarizability $\alpha = q_{\rm D}^2/k_{\rm D}$ is the same of the induced point dipole. We chose the value $q_{\rm D}=4.0e$ based on polarization energy evaluations of different Drude charges in various system configurations. This choice yielded a polarization energy of a test configuration of 2000 molecules that agrees within uncertainty with the original PJV-P potential. However, possibly because of the use of sPME in the present case, as opposed to reaction field in PJV-P, this result is 5% lower than that obtained in the limit of very large polarization charge. 45 Our choice was motivated by our aim of reproducing the polarization energy of the PJV-P model as a whole rather than just matching the point dipole limit. Further challenges in this parameterization included ensuring that the average displacement of the Drude site was large enough to be



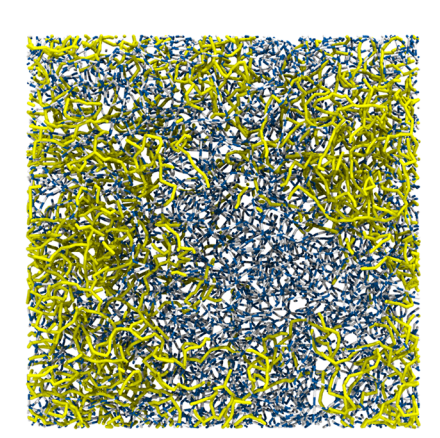




FIG. 1. Three simulation snapshots at, from left to right, 400, 380, and 300 K, and 926, 759 and 700 kg/m³, respectively. The largesst hydrogen-bonded cluster in the system is highlighted using thicker, yellow bonds. HF molecules not belonging to the largest cluster are shown as sticks with white (H) and blue (F) ends.

accurately represented on the sPME grid but not so large to become attracted and trapped within another molecule. In fact, a positive polarization charge tends to find its equilibrium position closer to the molecule's interior, improving stability.

In the following, we present the analysis of the percolation threshold as computed from molecular dynamics simulations of two systems (1000 and 8000 HF molecules, respectively) simulated at a number of different state points in the canonical ensemble, varying the temperature from 230 to 400 K and the density from 320 to 1010 kg/m³. Figure 1 shows the simulation snapshots taken at 400, 380, and 300 K, where the largest hydrogen-bonded cluster (computed as described later) is highlighted using thicker, yellow bonds. At 400 K, the largest cluster cannot span the entire system, and the hydrogen bond network is not percolating. At 380 K, the largest cluster is able to span the whole system but comprises only a small fraction of the molecules in the simulation box. Finally, at 300 K, the largest cluster is not only percolating but consists also of the majority of molecules in the system.

We performed the simulations using the GROMACS simulation package⁴⁶ version 2023.0 compiled in double precision to allow for an accurate minimization of the energy in the self-consistent field calculation for the induced dipoles. Note that a tight convergence criterion for the induced dipole calculation is necessary for an accurate evaluation of the virial.⁴⁷ We performed the data analysis using the MDAnalysis Python package.⁴⁸ The full input parameters, topology, and configurations are available online at https://doi.org/10.5281/zenodo.10783788.

RESULTS

The percolation transition refers to the critical point at which a system moves from one phase with isolated components to another, forming a large, connected cluster spanning the entire phase. In systems simulated using periodic boundary conditions, one can investigate the transition by calculating the probability of finding a cluster spanning the whole system as a function of the density (at constant temperature). By comparing the spanning probabilities for systems of different sizes, the percolation threshold is identified as the density where the probability curves for the two system sizes intersect, indicating the density at which a percolation pathway becomes sustainable across the system regardless of size. increasing system size, the transition happens in a narrower range of densities. In the thermodynamic limit, when crossing the percolation threshold, the system changes abruptly from zero percolation probability to one. Here, we consider a cluster to be spanning if it performs a closed loop across the periodic boundary conditions.

To perform this calculation, a criterion is needed to decide whether two HF molecules belong to the same cluster, that is to say, whether they are hydrogen-bonded or not. For this initial analysis, we require a pair of atoms H and F belonging to two different molecules to be within a given distance $d_{HB} = 2.38$ Å. The same distance d_{HB} is used for all thermodynamic points. This criterion is different form that used in the context of other hydrogen bonded liquids as it uses one distance only instead of two distances or one distance and one angle. In fact, the $H \cdot \cdot \cdot F$ coordination number computed up to the first minimum of the corresponding radial distribution function accounts for about 1.01 molecules. The distribution of the $F-H \cdot \cdot \cdot F$ angle is sharply peaked at 180° , where

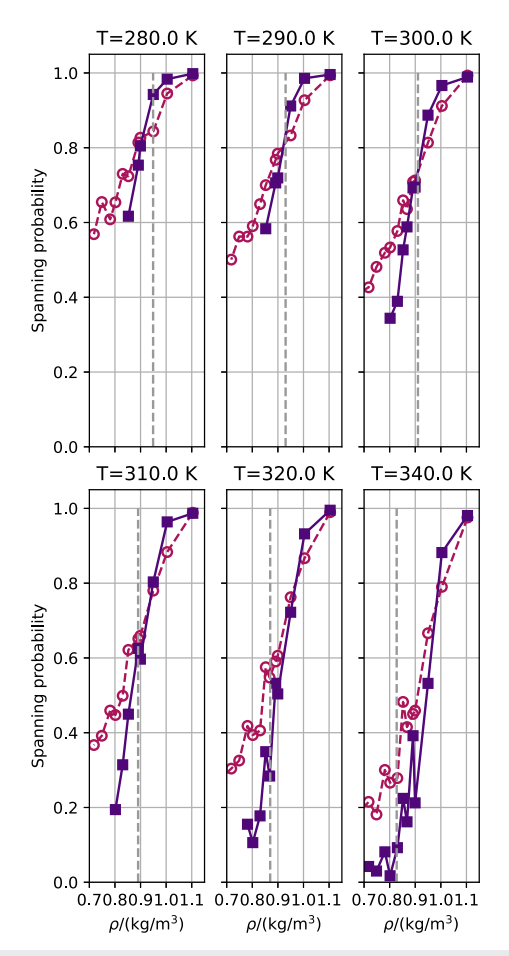


FIG. 2. Spanning probability curves as a function of the density, computed at six temperatures for the large (squares) and small (circles) systems. The vertical dashed line represents the liquid density of the model at the corresponding temperature along the coexistence line.

configurations below 150° are quite rare. ^{11,38} Therefore, the addition of an angular or a F–F distance criterion would be redundant.

The spanning probabilities shown in Fig. 2 are computed using this simple yet effective strategy. The squares and circles represent the spanning probability of the large and small systems, respectively. In addition, we report, as vertical dashed lines, the value of the liquid density at the same temperature but computed along the liquid-vapor coexistence line using explicit coexistence simulations. 45 Even though, as it will become apparent soon, this approach is not entirely correct or self-consistent, it shows that the percolation threshold density is located below the coexistence line at low temperatures (implying a percolating hydrogen-bond network in the fluid at coexistence) and above it at high temperatures (implying a non-percolating hydrogen-bonded network at coexistence). The percolation threshold is located around about 300 K. We will elaborate later on the significance of this finding. Note that the system can experience spontaneous separation into liquid and vapor at low enough densities, close to or beyond the spinodal line. In this case, the connectivity of the system improves, and there is a sudden jump in the spanning probability. This jump is more likely to happen in

the large systems, as they are less artificially stabilized by periodic boundary conditions than the smaller ones. We have excluded these data points from our analysis.

The issue with the present choice of the hydrogen-bonding criterion is that the length of the hydrogen bond between two HF molecules is known to depend on the state point. ⁴¹ In this sense, a fixed distance criterion to define whether two molecules share a hydrogen bond might not be the best choice. A common solution to this problem is using as d_{HB} the minimum in the F–H intermolecular radial distribution function that occurs right after the first peak, namely, the distance below which most of the first neighboring hydrogens are included.

Figure 3 shows the H-F radial distribution function as well as the contributions coming from the first, second, and third neighboring hydrogen atoms for a selected set of state points for the small system, along with the result of a quadratic fit used to locate the distance r_{\min} of the first minimum. It turns out that r_{\min} is not only state-dependent but also mildly size-dependent, being slightly different, under the same thermodynamic conditions, in the small and large systems. In addition, r_{\min} is clearly affected by the distribution of the second and third neighbors, so it is not necessarily a perfect proxy for the maximum hydrogen bond distance. In fact, the spanning probability curves computed using $d_{HB} = r_{\min}$ become quite noisy above the coexistence line, and it was possible to use only a smaller set of state points for this analysis. Nevertheless, in this case, the estimated percolation temperature crosses the coexistence line, too, even though it is slightly lower (around about 290 K) than the one obtained using the fixed cutoff criterion $d_{HB} = 2.38 \text{ Å}$. In Fig. 4, we report on the ρ -T plane the locus of the percolation threshold calculated using these two criteria, as well as the result of two more calculations with $d_{HB} = 2.36$ Å and $d_{HB} = 2.4$ Å. All four curves are close to each other in the neighborhood of the coexisting line, showing that, at least in this region, they provide the same picture of the existence and location of the percolation transition. The percolation threshold curves start spreading out in the region above the coexistence line, although they follow the same qualitative trend.

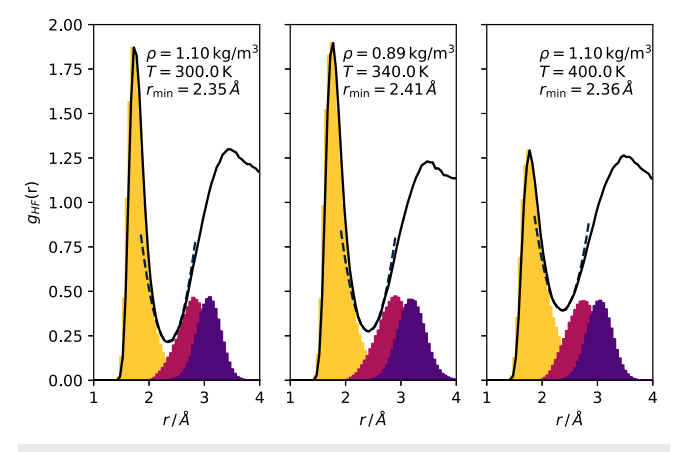


FIG. 3. Radial distribution functions measured at various state points of the F–H pairs (solid lines), including the contributions from first (yellow), second (plum), and third (purple) neighbors. The quadratic fit used to locate the minimum is also reported (dashed lines).

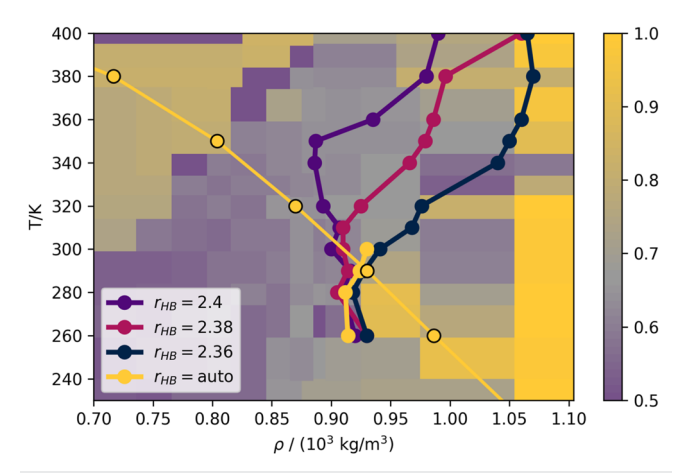


FIG. 4. Temperature—density phase diagram, including the location of the liquid branch of the coexistence line (yellow points with a black border), the calculated percolation transition curves using four different criteria (circles), and the value of the fraction f of the largest population in color code from purple (0.5) to yellow (1.0). The label auto corresponds to the criterion that uses the state-dependent cutoff.

All considered, these results seem to confirm the presence of a well-defined percolation threshold close to the coexistence line around 280–300 K. Interestingly enough, to the best of our knowledge, the other small associating liquid that is known to possess a hydrogen-bond percolation transition is water, which, however, is located in the supercritical region. ^{18,19}

Still, as noted before, the uncertainty in how to properly define the presence of a hydrogen bond calls for independent confirmation of this effect, or at least to correlate it with other changes in the properties of the liquid that do not depend on the hydrogen bond criterion. To this end, we have investigated the properties of the local density for structural changes upon crossing of the percolation threshold.

We obtained the local density distribution by counting the number of neighbors within a 6 Å distance from each fluorine atom. Since these volumes are fixed, the probability $p(\Delta N)$ of observing a fluctuation in the number of particles N within the volume can be expressed 52 as

$$p(\Delta N) \propto \exp\left[-\frac{(\Delta N)^2}{2k_BT}\left(\frac{\partial \mu}{\partial N}\right)_{V,T}\right],$$
 (1)

where k_B is Boltzmann's constant. This probability distribution is a Gaussian function of ΔN with a variance, $k_B T (\partial N/\partial \mu)_{V,T} = k_B T \rho N \chi_T$, which is proportional to the mean density ρ and isothermal compressibility χ_T .

Figure 5 shows the (non-normalized) particle number distributions for a selected number of state points, along with the result of the best fit to one and two Gaussian distributions. The upper left panel of Fig. 5 shows that at high densities and low temperatures, the distribution is unimodal and accurately described by a single Gaussian probability distribution over about six orders of magnitude. The contribution of the second Gaussian is about four orders of magnitude smaller and completely negligible. The local density

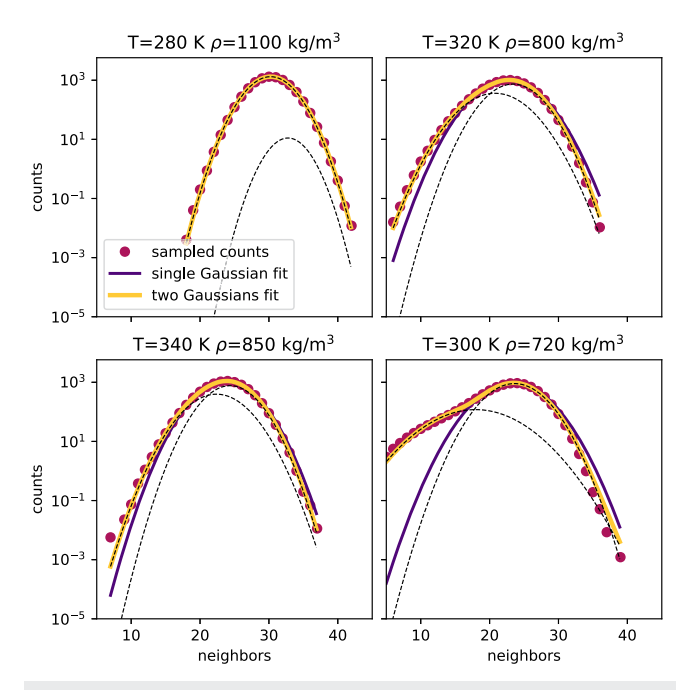


FIG. 5. Distribution of the local density at four different state points. This plot reports the counts (circles) of the number of neighboring fluorine atoms within a 6 Å distance from a central one. The solid lines represent the best fit to one (purple solid line) or two (yellow solid line) Gaussian distribution functions. The dashed lines represent the contribution of the two Gaussian functions in the bimodal fit. The complete set of distributions is available in the supplementary material.

fluctuations at this state point are characteristic of a single mean liquid density.

Not all the state points considered enjoy this feature. At higher temperatures and lower densities, but still in the liquid phase at 340 K and 850 kg/m³, the distribution is no longer unimodal, as the lower left panel of Fig. 5 shows. The superposition of two Gaussian distributions (yellow solid line) fits the sampled points better than a single Gaussian one (purple solid line). In this case, the fluid seems to be characterized by two distinct populations with their mean density and compressibility (linked to the width of the distribution). This situation is similar to a state point in the metastable region, in the upper right panel of Fig. 5, at 320 K and 800 kg/m³. Far away from the coexistence line, at 300 K and 720 kg/m³, the two Gaussians become increasingly separated. Note that in all cases, the Bayesian information criterion⁵³ strongly favors the bimodal distribution. In this sense, it is clear that the distributions are bimodal, and the critical quantity that needs to be determined is the contribution of each of the two modes to the total distribution.

The population fraction f_i of the ith distribution can be calculated using the amplitude, A_i , and standard deviation, σ_i , of the corresponding Gaussian, as $f_i = A_i \sigma_i / (A_1 \sigma_1 + A_2 \sigma_2)$, because the area under a Gaussian function is proportional to $A_i \sigma_i$. As a measure of the uni- or bimodality of the density distribution, we compute the parameter $f = \max(f_1, f_2)$, which ranges from 0.5 to 1.0. The case f = 1.0 corresponds to a unimodal distribution, whereas f = 0.5 corresponds to the case of two equally sized populations.

In Fig. 4, we use a color code to report the value of the fraction f. By comparing the location of the percolation threshold and the states with a unimodal distribution, one can notice some correlation between the two. The liquid with a unimodal distribution at high densities ($\rho > 1050 \text{ kg/m}^3$) and along the coexistence line from the highest density down to around about 900 kg/m³ is characterized by a percolating hydrogen bond network. The onset of the bimodal distribution, particularly along the coexistence line, seems to coincide with the transition to a non-percolating fluid. Following the coexistence line toward lower densities, one can notice that the value of f increases again.

This transition from high to low and eventually back again to high values of f could reflect the previously described structural change. At high densities, the system forms a tightly connected network of branched polymers. Once the percolation threshold is reached, the system transitions into an ensemble of polymers that are mainly bound via the van der Waals interaction. With increasing temperature, the density of chains becomes smaller, while the distance between hydrogen-bonded molecules cannot change much, thereby increasing its relative contribution to the local density. In other words, the increased prevalence of unimodality at high temperatures could be an effect of HF chains becoming gradually more separated. Here, we note that we have distinguished the two structurally different molecular environments only through their local density. More refined approaches that use the correlation between the molecular dipole moments or other suitably defined order parameters could lead to a more detailed description of the liquid structure.

CONCLUSIONS

Molecular dynamics simulations provided compelling evidence of a percolation transition in the hydrogen bond network of liquid HF. The percolation transition appears regardless of the criterion used to define hydrogen bonds, even though its exact location depends on it. The high connectivity region of the percolating fluid seems to be correlated with a unimodal distribution in the local densities. Instead, the low connectivity region with no percolating hydrogen bond network is characterized by a bimodal local density distribution at moderate temperatures, and a unimodal distribution peaked at low density at high temperatures. It should be emphasized that our results only reveal the existence of a percolation transition and not of a first-order liquid/liquid phase transition. The existence of two local structures with different densities is only a precondition for such a phase transition. In this sense, the present scenario could even be compatible with the presence of a liquid-liquid phase transition. A clarification of this point needs further investigations.

At the moment, we can only speculate on the possible microscopic origin of this behavior. One possible explanation comes to mind by regarding the liquid as a melt of (hydrogen-bonded) polymers. At a relatively low macroscopic density, the bimodality of the local density can reflect the coexistence of tightly bound neighboring molecules within a hydrogen-bonded chain and more loosely bound molecules belonging to neighboring chains, coordinated via van der Waals attraction. Another possibility is that because of the low surface tension of liquid HF, spontaneous cavitation effects could break the connectivity of the hydrogen bond network, leading to the

transition from a percolating to a non-percolating hydrogen-bonded fluid.

The implications of our study extend far beyond the confines of HF. They suggest a broader paradigm for interpreting the behavior of associating liquids, in particular regarding the presence of structural heterogeneities and their link with the system's connectivity. This could potentially influence the development of new models that can accurately predict fluid behaviors across a wider range of conditions.

SUPPLEMENTARY MATERIAL

See the supplementary material for the complete set of local density distributions.

ACKNOWLEDGMENTS

P.J. acknowledges the financial support from the Hungarian NKFIH Foundation under Project No. 134596.

AUTHOR DECLARATIONS

Conflict of Interest

The authors have no conflicts to disclose.

Author Contributions

Elija Feigl: Conceptualization (supporting); Investigation (equal); Writing – original draft (supporting). Pal Jedlovszky: Conceptualization (supporting); Investigation (equal); Writing – original draft (supporting). Marcello Sega: Conceptualization (lead); Investigation (equal); Writing – original draft (lead).

DATA AVAILABILITY

The data that support the findings of this study are openly available in Zenodo at http://doi.org/10.5281/zenodo.10783788.

REFERENCES

- ¹S. I. Hommeltoft, Appl. Catal., A 221, 421 (2001).
- ²A. T. Tabereaux and R. D. Peterson, *Treatise on Process Metallurgy* (Elsevier, 2014), pp. 839–917.
- ³ A. P. Ratvik, R. Mollaabbasi, and H. Alamdari, ChemTexts 8, 10 (2022).
- ⁴T. Hiyama, *Organofluorine Compounds: Chemistry and Applications* (Springer Science & Business Media, Berlin, 2013).
- ⁵D. M. Knotter, J. Am. Chem. Soc. **122**, 4345 (2000).
- ⁶P. Jedlovszky and R. Vallauri, Mol. Phys. 93, 15 (1998).
- ⁷A. Galindo, S. J. Burton, G. Jackson, D. P. Visco, and D. A. Kofke, Mol. Phys. **100**, 2241 (2002).
- ⁸S. A. Febra, A. Aasen, C. S. Adjiman, G. Jackson, and A. Galindo, Mol. Phys. 117, 3884 (2019).
- ⁹ A. Haghmoradi and W. G. Chapman, J. Chem. Phys. **150**, 174503 (2019).
- ¹⁰ A. Haghmoradi, B. D. Marshall, and W. G. Chapman, J. Chem. Eng. Data 65, 5743 (2020).
- ¹¹L. Pártay, P. Jedlovszky, and R. Vallauri, J. Chem. Phys. **124**, 184504 (2006).

- ¹² M. J. McGrath, I.-F. W. Kuo, and J. I. Siepmann, Phys. Chem. Chem. Phys. 13, 19943 (2011).
- ¹³ J. Friedrich, E. Perlt, M. Roatsch, C. Spickermann, and B. Kirchner, J. Chem. Theory Comput. 7, 843 (2011).
- ¹⁴E. Perlt, J. Friedrich, M. von Domaros, and B. Kirchner, Chem. Phys. Chem. 12, 3474 (2011).
- ¹⁵G. Bovolenta, S. Bovino, E. Vöhringer-Martinez, D. A. Saez, T. Grassi, and S. Vogt-Geisse, Mol. Astrophys. 21, 100095 (2020).
- ¹⁶E. A. Orabi and J. D. Faraldo-Gómez, J. Chem. Theory Comput. **16**, 5105 (2020).
- ¹⁷A. Oleinikova, I. Brovchenko, A. Geiger, and B. Guillot, J. Chem. Phys. 117, 3296 (2002).
- ¹⁸L. Pártay and P. Jedlovszky, J. Chem. Phys. **123**, 024502 (2005).
- ¹⁹ M. Bernabei, A. Botti, F. Bruni, M. A. Ricci, and A. K. Soper, Phys. Rev. E 78, 021505 (2008).
- ²⁰G. G. Simeoni, T. Bryk, F. A. Gorelli, M. Krisch, G. Ruocco, M. Santoro, and T. Scopigno, Nat. Phys. 6, 503 (2010).
- ²¹ P. Schienbein and D. Marx, Phys. Rev. E **98**, 022104 (2018).
- ²²I. Brovchenko, A. Krukau, A. Oleinikova, and A. K. Mazur, Phys. Rev. Lett. **97**, 137801 (2006)
- ²³ M. Sega, G. Horvai, and P. Jedlovszky, Langmuir 30, 2969 (2014).
- ²⁴M. Sega, G. Horvai, and P. Jedlovszky, J. Chem. Phys. **141**, 054707 (2014).
- ²⁵ J. Kolafa and I. Nezbeda, Mol. Phys. **72**, 777 (1991).
- ²⁶ J.-M. Caillol, J. Chem. Phys. **98**, 9835 (1993).
- ²⁷C. Holm and J.-J. Weis, Curr. Opin. Colloid Interface Sci. **10**, 133 (2005).
- ²⁸G. Ganzenmüller, G. Patey, and P. J. Camp, Mol. Phys. **107**, 403 (2009).
- ²⁹L. Rovigatti, J. Russo, and F. Sciortino, *Phys. Rev. Lett.* **107**, 237801 (2011).
- ³⁰L. Rovigatti, S. Kantorovich, A. O. Ivanov, J. M. Tavares, and F. Sciortino, J. Chem. Phys. 139, 134901 (2013).
- ³¹B. Smit, C. Williams, E. Hendriks, and S. D. Leeuw, Mol. Phys. **68**, 765 (1989).
- ³² M. Deraman, J. Dore, J. Powles, J. Holloway, and P. Chieux, Mol. Phys. 55, 1351 (1985).
- 33 W. L. Jorgensen and M. E. Cournoyer, J. Am. Chem. Soc. 100, 4942 (1978).
- 34 M. L. Klein, I. R. McDonald, and S. F. O'Shea, J. Chem. Phys. 69, 63 (1978).
- ³⁵M. E. Cournoyer and W. L. Jorgensen, Mol. Phys. **51**, 119 (1984).
- ³⁶W. L. Jorgensen, J. Am. Chem. Soc. **103**, 335 (1981).
- ³⁷P. Jedlovszky and R. Vallauri, Mol. Phys. **92**, 331 (1997).
- ³⁸P. Jedlovszky and R. Vallauri, J. Chem. Phys. **107**, 10166 (1997).
- ³⁹B. J. Howard, T. R. Dyke, and W. Klemperer, J. Chem. Phys. **81**, 5417 (1984).
- ⁴⁰W. Klopper, M. Quack, and M. A. Suhm, Chem. Phys. Lett. **261**, 35 (1996).
- ⁴¹T. Pfleiderer, I. Waldner, H. Bertagnolli, K. Tödheide, and H. E. Fischer, J. Chem. Phys. **113**, 3690 (2000).
- ⁴²P. Jedlovszky and R. Vallauri, J. Chem. Phys. **115**, 3750 (2001).
- ⁴³S. E. McLain, C. J. Benmore, J. E. Siewenie, J. J. Molaison, and J. F. C. Turner, J. Chem. Phys. **121**, 6448 (2004).
- ⁴⁴S. E. McLain, C. J. Benmore, J. E. Siewenie, J. Urquidi, and J. F. C. Turner, Angew. Chem. **116**, 1986 (2004).
- ⁴⁵E. Feigl, "Structure of the hydrogen fluoride liquid/vapour interface investigated using molecular dynamics simulations," M.S. thesis, University of Vienna, 2018, https://utheses.univie.ac.at/detail/46079.
- ⁴⁶ M. J. Abraham, T. Murtola, R. Schulz, S. Páll, J. C. Smith, B. Hess, and E. Lindahl, SoftwareX 1–2, 19 (2015).
- ⁴⁷ P. T. Kiss and A. Baranyai, "On the pressure calculation for polarizable models in computer simulation," J. Chem. Phys. **136**, 104109 (2012).
- ⁴⁸N. Michaud-Agrawal, E. J. Denning, T. B. Woolf, and O. Beckstein, J. Comput. Chem. 32, 2319 (2011).
- ⁴⁹ J.-P. Hovi and A. Aharony, *Phys. Rev. E* **53**, 235 (1996).
- ⁵⁰L. B. Pártay, P. Jedlovszky, I. Brovchenko, and A. Oleinikova, J. Phys. Chem. B 111, 7603 (2007).
- ⁵¹ J. Škvor, I. Nezbeda, I. Brovchenko, and A. Oleinikova, Phys. Rev. Lett. 99, 127801 (2007).
- ⁵² J. Hansen and I. Mc Donald, *Theory of Simple Liquids*, 3rd ed. (Academic Press, London, UK, 2006).
- ⁵³G. Schwarz, Ann. Stat. **6**, 461 (1978).